Robotica (2017) volume 35, pp. 206–223. © Cambridge University Press 2015
doi:10.1017/S0263574715000119

Complementary control for robots with actuator redundancy: an underwater vehicle application

Giovanni Indiveri* and Alessandro Malerba

Dipartimento Ingegneria Innovazione, Università del Salento, via Monteroni, 73100 Lecce, Italy

(Accepted February 9, 2015. First published online: March 6, 2015)

SUMMARY

Complementary filtering is a frequency based method used to design data processing algorithms exploiting signals with complementary spectra. The technique is mostly used in sensor fusion architectures, but it may also be effective in the design of state estimators. In spite of its potential in several areas of robotics, the complementary filtering paradigm is poorly used as compared to alternative time domain methods. The first part of the paper aims at reviewing the basics of complementary filtering in sensor data processing and linear systems state estimation. The second part of the paper describes how to exploit the main ideas of complementary filtering to design a depth controller for an actuator redundant autonomous underwater vehicle (AUV). Unlike with alternative state space methods commonly used to address the design of control solutions for actuator redundant systems, the proposed approach allows to fully exploit the knowledge of frequency characteristics of actuators. Simulation results are reported to demonstrate the effectiveness of the proposed solution.

KEYWORDS: Redundant actuation robot control; Marine systems; Motion control; Robot control; Autonomous vehicles; Complementary filtering.

1. Introduction

Actuator redundancy refers to the situation where more actuators are used to control a given degree of freedom. Contrary to kinematics redundancy, where a number of internal motions are possible to achieve the same task space objective, actuator redundancy does not increase the robot mobility. Actuator redundancy in mechanical systems can be exploited to optimize the mechanical design.[9] In serial link manipulators actuator redundancy can be used to increase the range of end-effector impedance or to produce a maximum end-effector force in a more homogeneously distributed way.[13] Vehicles are also occasionally equipped with redundant actuation systems: in the vast majority of practical situations, the strategy on how to exploit each available actuator is chosen either by (a) solving a control problem taking explicitly into account the presence of multiple actuators (usually within an optimal control framework) or by (b) computing the overall needed control effort and subsequently distributing such effort on the available actuators. This latter problem is known as *control allocation* that is quite relevant in marine applications.[15] For a comparative review about the two possible strategies (a) and (b) refer to ref. [7] and to the references therein: a common feature to these known solutions is that they are derived based on a state space modeling of the system dynamics that does not allow to easily account for the frequency characteristics of the actuators.

In this paper, we describe a frequency based method to solve an actuator redundancy problem in the presence of actuators with different spectral characteristics: in particular, we present the design of a controller for the heave of an underwater vehicle equipped with two actuation systems for this same degree of freedom. To the best of our knowledge the proposed approach is novel and original: contrary to alternative state space methods it allows to easily account for the known spectral properties of the actuators through a straightforward frequency based design. The proposed solution builds on the idea of complementary filtering. Complementary filtering is a classical frequency method widely

* Corresponding author. E-mail: giovanni.indiveri@unisalento.it

https://doi.org/10.1017/S0263574715000119 Published online by Cambridge University Press

adopted, for example, in navigation and guidance applications[10] of flying robots and vehicles. In essence, in most applications it consists in combining sensor signals with complementary spectra to recover an estimate of a desired quantity. In spite of its relevance, complementary frequency based methods are seldom exploited in robotics applications. The aim of this work is hence twofold: first the basics of complementary filtering methods, including linear state estimation, are briefly reviewed. Then, the paradigm of complementary filtering is applied to design a novel heave controller for an actuator redundant underwater vehicle. Indeed, the idea of complementary filtering can be extended to the design of control systems characterized by the availability of multiple actuators with different bandwidths: this may be the case of redundant robots as the AUV Folaga considered in this work.

As a result of the proposed approach (called *complementary actuation* in the following) the heave control force is seemingly generated by the concurrent operation of the two available actuation systems each working in its most natural frequency spectrum. This approach can be applied to virtually any actuator redundant robotic system having actuators with complementary bandwidths.

As for the specific application on the heave control of an AUV, notice that automatic depth control is one of the most basic, yet fundamental, functionalities of underwater vehicles. The task of heave control is particularly important for autonomous underwater robots that are been employed in an increasing number of application scenarios. Since the early work described in Ref. [5] many different control design methods and technologies have been applied to the problem: basic PID-based solution are described, by example, in refs. [17], [3] and [1] while a gain-scheduling approach is addressed in ref. [14]. A model predictive control (MPC) design for the depth regulation of an underwater robot was more recently illustrated and discussed in ref. [16]. The modeling of heave dynamics of underwater vehicles together with possible control solutions is also covered in ref. [6].

Unlike most of the problems concerning underwater vehicles considered in the literature, this work addresses the problem of depth control for a vehicle equipped with two separate actuation systems for the heave axis: a ballast tank system and a set of four jet motors generating vertical forces in the bow and stern of the vehicle. The vehicle at hand is the AUV Folaga described in ref. [4]. The two actuation systems for the heave axis have different time constants: the ballast tank system is rather slow, while the jet actuators have a much faster dynamics. The vehicle's factory designed control system exploits either the ballast tank system or the vertical thrusters for heave command according to the mission specification, but never concurrently. Pure vertical dive maneuvers (i.e. at zero surge) are typically controlled by the ballast tank system only while during via point navigation depth is regulated using the vertical thrusters. The proposed solution aims at designing a control system able to concurrently exploit both actuator systems using them in their natural frequency domain. In particular, the designed controller is inspired by the theory of complementary filtering in estimation where the output of slow sensors (low-pass filters) is combined with the output of faster sensors (or the very plant model, i.e. high-pass filters) to generate an estimate. In the given setting a depth controller is designed generating a desired force command. This signal is partitioned in a lower and higher frequency component: the former is sent to the ballast tank system and the latter to the jet thruster actuators. As a result, the depth force command is seemingly executed concurrently by the two actuation systems. Preliminary results relative to the complementary control of an AUV have already been presented in ref. [12]. Here we extend that work by adding a review of complementary methods in estimation and filtering and a literature overview of redundant actuation approaches. Moreover, we include a stability analysis as well as additional simulation results to analyze the performance of the proposed approach.

Section 2 gives a brief overview of the complementary filtering technique and its extension to actuation as adopted in the paper. The AUV depth model used for control design is illustrated in Section 3 while the resulting control solution is presented in Section 4. Simulation results are reported in Section 5 while conclusion are finally addressed in Section 6.

2. Complementary Methods: Filtering and Actuation

2.1. Output signal complementary filtering

In general, complementary filters provide a means to fuse multiple independent noisy measurement of the same signal that have complementary spectral characteristics. Consider a signal $x(t)$ in the time domain and the related measurements $y_k(t)$ for $k = 1, 2, \ldots, N$ coming from different sensors.

https://doi.org/10.1017/S0263574715000119 Published online by Cambridge University Press

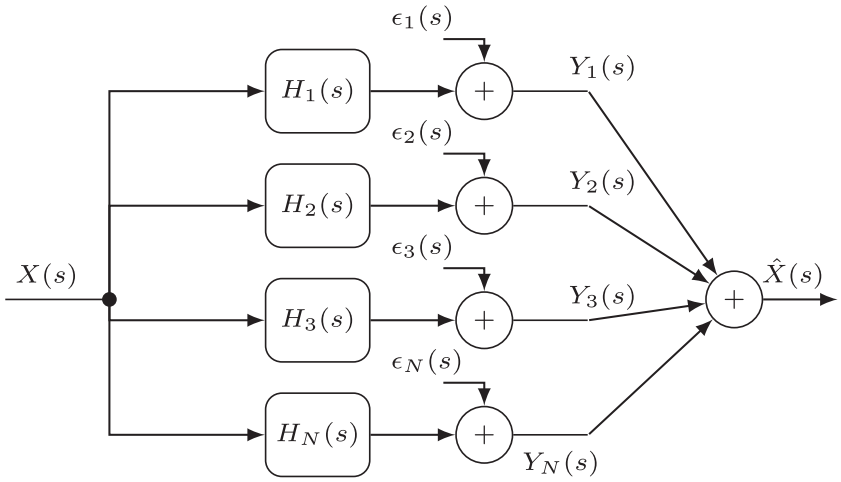


Fig. 1. Basic complementary filter for estimation.

Assuming the sensor models to be linear, in the Laplace domain the following would hold (refer to Fig. 1):

$$Y_k(s) = H_k(s)X(s) + \epsilon_k(s), \tag{1}$$

where $H_k(s)$ is the transfer function of the kth sensor and $\epsilon_k(s)$ is the corresponding measurement noise. Consider N proper transfer functions $P_k(s)$ for $k = 1, \ldots, N$ such that

$$\sum_{k=1}^{N} P_k(s)Y_k(s) = \left(\sum_{k=1}^{N} P_k(s)H_k(s)\right) X(s) + \sum_{k=1}^{N} P_k(s)\epsilon_k(s). \tag{2}$$

If the weights $P_k(s)$ are chosen such that

$$\sum_{k=1}^{N} P_k(s)H_k(s) = 1 \quad \Longrightarrow \tag{3}$$

$$\sum_{k=1}^{N} P_k(s)Y_k(s) = X(s) + \sum_{k=1}^{N} P_k(s)\epsilon_k(s), \tag{4}$$

and assuming $P_k(s)$ and $\epsilon_k(s)$ to have orthogonal spectra for all k, i.e. $P_k(s)\epsilon_k(s) = 0 \; \forall \, k = 1, \ldots, N$ or, at least, that

$$P_k(s)\epsilon_k(s) \approx 0, \quad \forall \, k = 1, \ldots, N, \tag{5}$$

the unknown signal $X(s)$ could be estimated according to

$$\hat{X}(s) = \sum_{k=1}^{N} P_k(s)Y_k(s). \tag{6}$$

Notice that the complementary estimator in Eq. (6) builds on the fundamental *complementary condition* $\sum_{k=1}^{N} P_k(s)H_k(s) = 1$ in Eq. (3).

2.2. State space complementary filtering

Interestingly, the complementary filtering paradigm can be extended over to state space representations of linear systems to accomplish state estimation. Consider a vector $\mathbf{x}(t) \in \mathbb{R}^n$ depending on time t

https://doi.org/10.1017/S0263574715000119 Published online by Cambridge University Press

having Laplace transform $\mathcal{L}[\mathbf{x}(t)] = \boldsymbol{X}(s)$ and state equation

$$\dot{\mathbf{x}}(t) = A\,\mathbf{x}(t) + B\,\mathbf{u}(t), \tag{7}$$

for a known input $\mathbf{u}$. Given a gain matrix $L \in \mathbb{R}^{n\times n}$ consider the identity

$$\boldsymbol{X}(s) = (s I_n + L)^{-1}\,(s I_n + L)\,\boldsymbol{X}(s), \tag{8}$$

being I_n the identity matrix of size n. Equation (8) can be used to design a state estimator by viewing the left-hand side of it as an estimate of $\boldsymbol{X}(s)$ and the right-hand side as being related to available measurements. In particular, assuming that a linear measurement $\mathbf{y}(t) \in \mathbb{R}^m : \mathcal{L}[\mathbf{y}(t)] = \boldsymbol{Y}(s)$ is available such that

$$\mathbf{y}(t) = C\,\mathbf{x}(t) + D\,\mathbf{u}(t), \tag{9}$$

$$\boldsymbol{Y}(s) = C\,\boldsymbol{X}(s) + D\,\boldsymbol{U}(s), \tag{10}$$

the complementary condition

$$(s I_n + L)^{-1}\,(s I_n + L) = (s I_n + L)^{-1}\,s I_n + (s I_n + L)^{-1}\,L = I_n, \tag{11}$$

leads to rewriting Eq. (8) as

$$\hat{\boldsymbol{X}}(s) = (s I_n + L)^{-1}\,s\boldsymbol{X}(s) + (s I_n + L)^{-1}\,L\boldsymbol{X}(s) \implies \tag{12}$$

$$(s I_n + L)\,\hat{\boldsymbol{X}}(s) = s\boldsymbol{X}(s) + L\boldsymbol{X}(s). \tag{13}$$

By viewing the right-hand side of Eq. (13) as being related to measurements, the gain matrix L is factorized as

$$L = KC, \tag{14}$$

where $C \in \mathbb{R}^{m\times n}$ is the output matrix in Eq. (9) and $K \in \mathbb{R}^{n\times m}$ is a gain matrix to be defined. In the time domain Eq. (13) corresponds to

$$\dot{\hat{\mathbf{x}}}(t) + KC\hat{\mathbf{x}}(t) = \dot{\mathbf{x}}_{meas}(t) + KC\mathbf{x}(t) \implies \tag{15}$$

$$\dot{\hat{\mathbf{x}}}(t) + KC\hat{\mathbf{x}}(t) + KD\mathbf{u}(t) = \dot{\mathbf{x}}_{meas}(t) + KC\mathbf{x}(t) + KD\mathbf{u}(t) \tag{16}$$

$$\dot{\hat{\mathbf{x}}}(t) + K\hat{\mathbf{y}}(t) = \dot{\mathbf{x}}_{meas}(t) + K\mathbf{y}(t) \tag{17}$$

$$\dot{\hat{\mathbf{x}}}(t) = \dot{\mathbf{x}}_{meas}(t) + K\,(\mathbf{y}(t) - \hat{\mathbf{y}}(t))\,, \tag{18}$$

where the "estimated output"

$$\hat{\mathbf{y}}(t) := C\hat{\mathbf{x}}(t) + D\mathbf{u}(t), \tag{19}$$

has been introduced and the variable $\dot{\mathbf{x}}_{meas}$ refers to a "measurement" of the time derivative of the state. Finally, notice that in the absence of sensors for experimentally acquiring $\dot{\mathbf{x}}_{meas}$, the "measured" value of the state derivative can be eventually generated by a "virtual" sensor based on the knowledge of the plant model Eq. (7). In particular, this would naturally lead to

$$\dot{\mathbf{x}}_{meas}(t) := A\,\hat{\mathbf{x}}(t) + B\,\mathbf{u}(t), \tag{20}$$

that in conjunction with Eq. (18) leads to the celebrated prediction/correction Luenberger state estimator

$$\dot{\hat{\mathbf{x}}}(t) = A\,\hat{\mathbf{x}}(t) + B\,\mathbf{u}(t) + K\,(\mathbf{y}(t) - \hat{\mathbf{y}}(t))\,. \tag{21}$$

https://doi.org/10.1017/S0263574715000119 Published online by Cambridge University Press

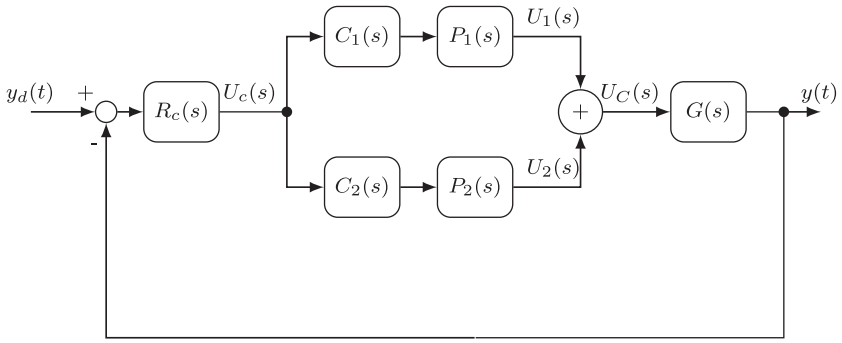


Fig. 2. A simple complementary actuation diagram for only two actuators.

As known, the state estimate $\hat{\mathbf{x}}$ defined by Eq. (21) will exponentially converge to the true state $\mathbf{x}$ as long as all the unobservable modes of A are asymptotically stable and, assuming (A, C) to be detectable, the Luenberger gain K is chosen such that the eigenvalues of $A - KC$ have strictly negative real part. Yet the point here is to illustrate the complementary filter interpretation of the Luenberger filter in Eq. (21): the Laplace domain definition of the Luenberger state estimate in Eq. (12) together with the definition of the model based "virtual" measurement in Eq. (20) lead to

$$\hat{\boldsymbol{X}}(s) = \left\{(s I_n + KC)^{-1}\, s\right\} \mathcal{L}\left[\mathbf{x}_{model}(t)\right] + \left\{(s I_n + KC)^{-1}\, K\right\} (\boldsymbol{Y}(s) - D\boldsymbol{U}(s)) \tag{22}$$

$$\mathbf{x}_{model}(t) := \int_0^t A\, \hat{\mathbf{x}}(\tau) + B\, \mathbf{u}(\tau)\, d\tau, \tag{23}$$

namely $\hat{\boldsymbol{X}}(s)$ can be viewed as the result of the combination of a *high-pass* filter

$$(s I_n + KC)^{-1}\, s,$$

of the model (state equation) and a *low-pass* filter

$$(s I_n + KC)^{-1}\, K,$$

of the measurement channel. This frequency based interpretation of the Luenberger filter is very well known[10] to practitioners that are aware (sometimes unconsciously) of the need to select the gain K with the double goal of guaranteeing stability of $A - KC$ while also modulating the frequency content of the measurement channel (correction) with respect to the model based estimate $\mathbf{x}_{model}(t)$ in Eq. (23) (prediction). The described frequency based interpretation of Luenberger filter is fully exploited in the stochastic framework of the Kalman filter where Gaussian noise is also considered on the state and measurement equations: the asymptotic (time invariant) Kalman filter can be thus viewed as a special complementary (Luenberger) filter[8] where the cut-off frequencies (i.e. the poles of $A - KC$) of the low-pass and high-pass filters defining the state estimate are optimally selected to minimize the covariance of the estimate.

Notice that the paradigm of complementary filtering can be extended over to nonlinear state estimation settings. A relevant and interesting application has been described in ref. [11] where a complementary filter is designed on $SO(3)$ for attitude estimation of a vehicle.

2.3. Complementary actuation

Assuming to have a process where an output can be controlled through more actuators, the idea of *complementary actuation* is to distribute the control effort over the actuators according to their spectral properties. Namely, the very principle of complementary filtering is exploited on the dual case of actuation. In particular, consider m actuators for the same degree of freedom. Figure 2 refers to the case $m = 2$ that corresponds to the situation at hand. In Fig. 2 the term $R_C(s)$ is a controller for the system $G(s)$, $P_h(s)$ are weights used to distribute the control effort on the various actuators, and finally, the terms $C_h(s)$ model the actuators.

https://doi.org/10.1017/S0263574715000119 Published online by Cambridge University Press

Given the plant model

$$Y(s) = G(s)U_C(s), \tag{24}$$

its input $U_C(s)$, following the set up depicted in Fig. 2, can be written as follows:

$$U_C(s) = \sum_{h=1}^{m} U_h(s), \tag{25}$$

where $U_h(s)$ is defined as

$$U_h(s) = C_h(s)P_h(s)R_C(s)\left[Y_d(s) - Y(s)\right], \tag{26}$$

being $Y_d(s)$ is the Laplace's transform of the reference signal. The term $U_C(s)$ is finally

$$U_C(s) = \left(\sum_{h=1}^{m} C_h(s)P_h(s)\right) R_C(s)\left[Y_d(s) - Y(s)\right], \tag{27}$$

that can be equated to its definition

$$U_C(s) = R_C(s)\left[Y_d(s) - Y(s)\right], \tag{28}$$

implying for the weights $P_h(s)$ that they must satisfy the (actuation) complementary condition

$$\sum_{h=1}^{m} C_h(s)P_h(s) = 1. \tag{29}$$

Overall, the closed loop system results in

$$Y(s) = G(s)\left(\sum_{h=1}^{m} C_h(s)P_h(s)\right) R_C(s)\left[Y_d(s) - Y(s)\right]. \tag{30}$$

2.3.1. Stability analysis. By direct inspection of the proposed control schema in Eqs. (29) and (30), it follows that sufficient conditions for closed loop bounded input bounded output (BIBO) stability are that

(s1) $\frac{G(s)R_C(s)}{1+G(s)R_C(s)}$ is BIBO stable,
(s2) $C_h(s)$ and $P_h(s)$ $\forall\, h \in [1, m]$ are stable, i.e. they do not have unstable poles.

Condition (s1) is of course also necessary, while condition (s2) is not necessary in a strict sense: indeed, if (s2) should be violated being condition (29) valid, there would be internal cancelations of unstable poles in the sum $\sum_{h=1}^{m} C_h(s)P_h(s) = 1$. In case these cancelations should be perfect (which is of course impossible in practice), condition (s1) would still guarantee BIBO stability of the overall closed loop system. Yet this situation is not possible in real applications as perfect internal cancelations never occur. Moreover, even if they should occur, there would be unstable natural responses associated to the unstable poles of $C_h(s)$ or $P_h(s)$. It thus follows that condition (s2) is also a practical necessity.

In order for the overall closed loop system $Y(s)/Y_d(s)$ to have a stable zero input (i.e. natural) response there shall not be any internal cancelations of unstable poles in $G(s)$, $R_C(s)$ and in the forward branch $G(s)R_C(s)$. Finally, notice that all transfer functions in conditions (s1) and (s2) need to be proper (i.e. either strictly proper or biproper).

https://doi.org/10.1017/S0263574715000119 Published online by Cambridge University Press

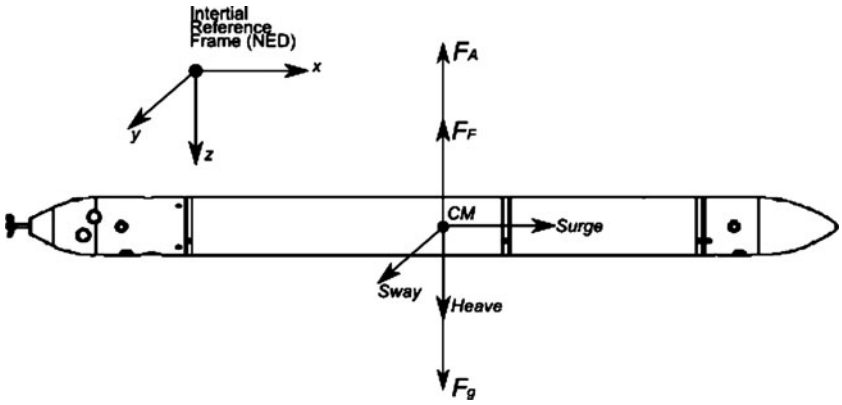


Fig. 3. Heave force balance: CM is the center of mass, F_A is due to buoyancy (Archimedes' force), F_F to viscous friction and F_g to gravity.

3. AUV Heave Model

The proposed control solution is designed for the slender body AUV (Fig. 3) called Folaga described in ref. [4]. The dynamic equations of this vehicle can be written as follows:

$$(M_I + M_A + m(t))\ddot{z}(t) = -\beta\dot{z}(t) + (M_I + m(t))g - \nabla\rho g + u_2(t), \tag{31}$$

and

$$\dot{m}(t) = -k\, m(t) + u_1(t), \tag{32}$$

where

M_I	Inertial mass of the vehicle.
M_A	Added mass.
$m(t)$	Mass of the fluid in the ballast tank at time t.
z	Depth of the vehicle.
β	Viscous friction coefficient in direction of z.
g	Gravity acceleration.
∇	Displacement.
ρ	Fluid density.
k	Inverse of the time constant of the ballast tank.
$u_1(t)$	Ballast tank control input.
$u_2(t)$	Heave control force generated by the electrical motors.

Equation (31) is relative to Newton's law along the heave axis[6] while Eq. (32) models the dynamics of the fluid in the ballast tank. Notice that Eq. (32) is indeed an approximation of the ballast tank fluid dynamics: the in- and out-flows from the tank will actually have different time constants as the inflow is governed by a simple valve (the water entering the tank due to the higher pressure of environmental water) while the outflow is generated by an active pump. Moreover, both the input and output flows of the ballast tank fluid will depend on the depth of the vehicle. Yet for control design purposes, the ballast fluid mass is modeled with the simple linear first order equation in Eq. (32) that neglects these details.

Equations (31)–(32) imply

$$[M_A + M_I + m(t)]\dddot{z}(t) + \ddot{z}(t)[u_1(t) - km(t) + \beta] = [u_1(t) - km(t)]g + \dot{u}_2(t), \tag{33}$$

that is nonlinear due to the terms $m(t)$ and $u_1(t)$ multiplying the derivatives of $z(t)$: yet notice that $M_I + M_A \in [50, 100]$Kg while $m(t) \in [0, 0.5]$Kg, namely $m(t) \ll (M_I + M_A)$ implying that Eq. (31) can be approximated by the linear dynamics

$$(M_I + M_A)\ddot{z}(t) = -\beta\dot{z}(t) + (M_I + m(t))g - \nabla\rho g + u_2(t). \tag{34}$$

https://doi.org/10.1017/S0263574715000119 Published online by Cambridge University Press

Equations (32) and (34) allow to derive the transfer function model

$$\tilde{M} := M_A + M_I \tag{35}$$

$$\delta := (M_I - \nabla\rho)g \tag{36}$$

$$Z(s) = \frac{1}{s(\tilde{M}s + \beta)}\left(\frac{g}{(s+k)}U_1(s) + U_2(s)\right) + \frac{\delta}{s^2(\tilde{M}s + \beta)}, \tag{37}$$

that corresponds to the structure in Eqs. (24)–(25) noticing that

$$G(s) = \frac{1}{s(\tilde{M}s + \beta)}, \tag{38}$$

and

$$\begin{aligned} U_C(s) &= \frac{g}{(s+k)}U_1(s) + U_2(s) \\ &= C_1(s)\,U_1(s) + C_2(s)\,U_2(s), \end{aligned} \tag{39}$$

being

$$C_1(s) = \frac{g}{(s+k)}, \quad C_2(s) = 1. \tag{40}$$

The last term on the right-hand side of Eq. (37) can be interpreted as a disturbance (matched with $U_C(s)$) that is null in case of perfectly neutral calibration, i.e. $M_I = \nabla\rho$.

4. Control Design

4.1. Controller

With reference to the model in Eqs. (37)–(40), a possible simple controller for $U_C(s)$ in Eq. (28) able to reject the matched disturbance δ in Eq. (36) is a proportional, integral and derivative (PID) controller

$$R_{PID} = K_{PID}\,\frac{(1+18s)(1+20s)}{s(s+1)} = \frac{U_C(s)}{Y_d(s) - Y(s)} = R_C(s), \tag{41}$$

to be eventually implemented through an anti-windup architecture.[2] Given the plant structure $G(s)$ in Eq. (38), a PID controller is sufficient to guarantee closed loop stability with a sufficiently large phase margin. The design can be performed in a straightforward fashion through standard frequency based loop shaping. The details of the design are here omitted for the sake of brevity. We only report that the PID gain K_{PID} has been selected as $K_{PID} = 7.63 \cdot 10^{-2}$ resulting in a phase margin of approximately 80°. Once the PID controller is defined, the weight functions $P_1(s)$ and $P_2(s)$ need to be determined in order to distribute the control signal $U_C(s)$ on the two available actuation systems.

As for the design of the spectral weight functions $P_1(s)$ and $P_2(s)$, given that the thrusters should be preferably used for the high frequency command components only, the corresponding spectral weight $P_2(s)$ is chosen to be a second order high-pass filter

$$P_2(s) = \left(\frac{\tau_f s}{1 + \tau_f s}\right)^2. \tag{42}$$

https://doi.org/10.1017/S0263574715000119 Published online by Cambridge University Press

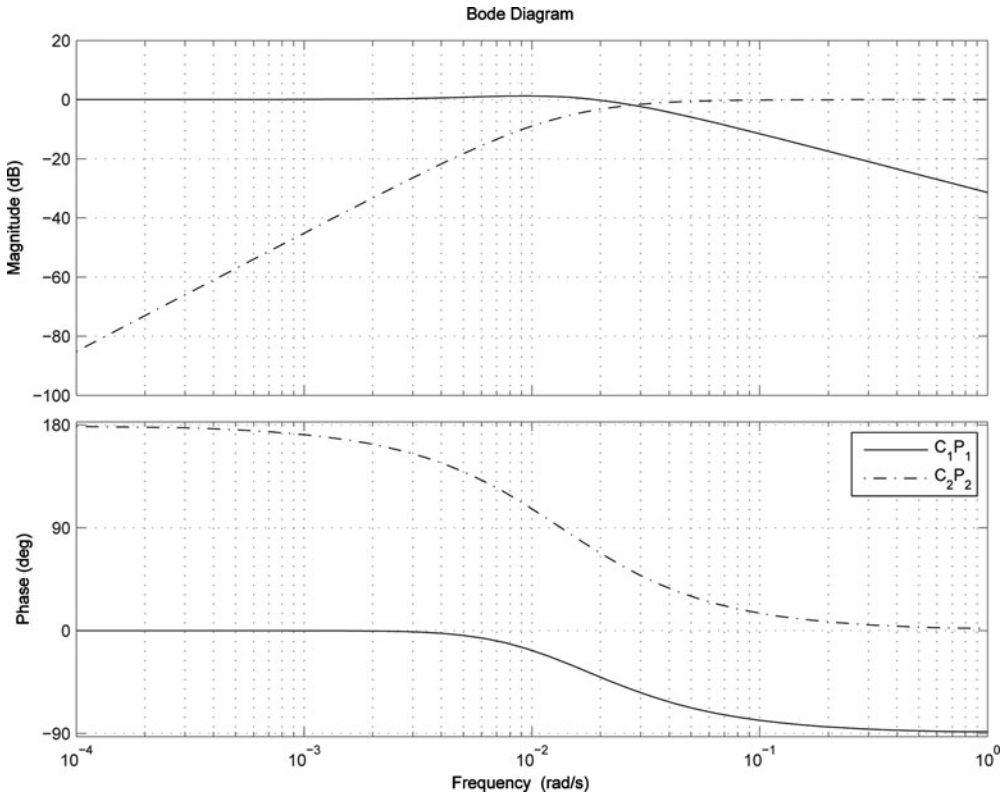


Fig. 4. Bode plots of $C_1(s)P_1(s)$, low-pass filter, and $C_2(s)P_2(s)$, high-pass filter.

Having defined $P_2(s)$ the spectral weight $P_1(s)$ for the ballast tank command follows directly from the complementary condition (29) resulting in the following:

$$P_1(s) = \frac{(2\tau_f s + 1)(s + k)}{g(1 + \tau_f s)^2}. \tag{43}$$

The parameter τ_f plays a fundamental role as it determines the threshold frequency identifying the low frequency region for the ballast tank control system as opposed to the high frequency region for the electric thrusters. Notice that this is exactly the counterpart of the situation in complementary filtering and, to some extent, in Kalman filtering. Indeed, the Kalman filter can be interpreted as a special complementary filter[8] where the lower frequency measurement information is combined with the higher frequency model dynamics information to generate the Kalman state estimate.

The k parameter in Eqs. (32) and (43) is $k = 8 \cdot 10^{-3}$ Hz while g is the gravity acceleration $g = 9.81$ m/s^2 and the τ_f parameter has been selected as $\tau_f = 81.76$ s. The Bode plots of $C_1(s)P_1(s)$ and $C_2(s)P_2(s)$ are reported in Fig. 4 showing the complementary behavior of the thruster and ballast tank commands.

Notice that the resulting transfer functions $P_1(s)$, $P_2(s)$, $C_1(s)$, $C_2(s)$, $R_C(s)$ and $G(s)$ in Eqs. (38), (40)–(43) satisfy the stability conditions described in Section 2.3.1.

4.2. Implementation issues

The proposed solution has been coded for experimental validation and simulation analysis. The presence of the integral action in Eq. (41) is necessary to reject the action of the matched disturbance δ defined in Eq. (36): yet given the limited capacity of the ballast tank and the relatively low power of the vertical thrusters, the integral action in the PID controller is likely to trigger actuation saturations. In order to cope with this, an anti-windup implementation of the PID controller has been realized.[2] In particular, the block diagram of the implementation is depicted in Fig. 5. where $A(s)$ and $B(s)$ are

https://doi.org/10.1017/S0263574715000119 Published online by Cambridge University Press

Table I. Simulation parameters.

M_I	38.8	Kg
M_A	41.83	Kg
β	12.26	N s/m
ρ	1025	Kg/m^3
$\bar{u}_1$	$1.5 \cdot 10^{-2}$	Kg/s
$\bar{u}_2$	3.43	N

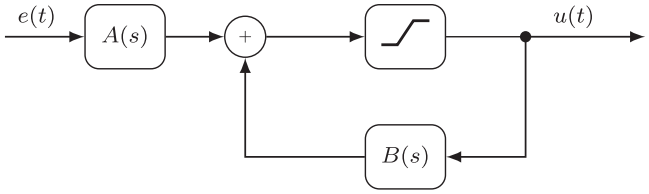


Fig. 5. The schema of anti-windup implementation used in this work.

defined as

$$A(s) = \frac{N_{PID}(s)}{\Gamma(s)} \tag{44}$$

$$B(s) = \frac{\Gamma(s) - D_{PID}(s)}{\Gamma(s)}, \tag{45}$$

being $N_{PID}(s)$ and $D_{PID}(s)$ the numerator and denominator respectively of the PID controller R_{PID} in Eq. (41). The $\Gamma(s)$ term is a polynomial in s with roots strictly lying in the left-hand side complex plane and such that $\Gamma(0) > 0$. $\Gamma(s)$ is designed such that $B(s)$ is proper (namely it has to be of order larger or equal to $D_{PID}(s)$) and with sufficiently fast poles with respect to the dynamics of the error variable feeding $A(s)$. Notice that given that $D_{PID}(s)$ has a pole in the origin it follows that $B(0) = 1$ that is essential to obtain the anti-windup behavior of the system. For the details about the functioning of this schema as an anti-windup device refer to ref. [2]. In the present case the $\Gamma(s)$ polynomial has been designed as $\Gamma(s) = (s + 1)^2$.

5. Simulation Results

The proposed complementary based solution for controlling the heave degree of freedom of the Folaga AUV has been extensively analyzed through numerical simulations. The controller illustrated in Section 4 has been coded in Matlab Simulink together with the full nonlinear vehicle model given by Eqs. (31)–(32). In particular, the ballast chamber $u_1(t)$ and thrusters $u_2(t)$ commands resulting from $R_{PID}(s)C_1(s)P_1(s)\,(Y_d(s) - Y(s))$ and $R_{PID}(s)C_2(s)P_2(s)\,(Y_d(s) - Y(s))$, respectively have been used as inputs to the full nonlinear model in Eqs. (31)–(32). Both the ballast chamber command $u_1(t)$ and the thrusters command $u_2(t)$ have been saturated in the range $[-\bar{u}_h, \bar{u}_h] \;:\; h = 1, 2$ as

$$u_h(t) \longrightarrow u_h(t)\sigma_h \quad : \quad \sigma_h = \begin{cases} 1 & |u_h(t)| < \bar{u}_h \\ \dfrac{\bar{u}_h}{|u_h(t)|} & \text{otherwise} \end{cases} \qquad h = 1, 2. \tag{46}$$

Indeed such saturation conditions reflect one of the most relevant aspects of the actuator systems being considered. The simulation parameters, on top of the ones already reported in the previous sections, are listed in table I.

https://doi.org/10.1017/S0263574715000119 Published online by Cambridge University Press

The reported simulations results refer to three kind of diving maneuvers which are as follows:

1. A sinusoidal depth reference with an amplitude of 7 meters for the first half of the task and of 5 meters during the second half.
2. A ramp depth reference.
3. A change of depth through a ramp as described in ref. [3].

This last reference is given by

$$z_d(t) = \begin{cases} 5 & \text{if } t \in [0; 100]\ s \\ 5 - 0.04(t - 100) & \text{if } t \in]100; 200[\ s \\ 1 & \text{if } t \in [200; 300]\ s, \end{cases} \tag{47}$$

and corresponds to a common motion task for underwater robotic vehicles.[3] The above simulations allow to evaluate the performance of the proposed solution. In particular, they illustrate that the use of the ballast chamber tank actuation system in the low frequency range of the depth PID controller results in an automatic buoyancy calibration. Namely, the ballast chamber in steady state when the depth reference is constant over a sufficiently long interval fills up to a level that makes δ in Eq. (36) tend to zero (neutral buoyancy condition, i.e. the weight $g(M_I + m(t))$ of the vehicle is compensated by buoyancy $g\nabla\rho$). Indeed in all the reported simulations the vehicle was initially positively buoyant, namely $g\nabla\rho > g(M_I + m(t)|_{t=0})$ resulting in a tendency of the vehicle to surface. Given the model parameters the neutral buoyancy condition is achieved when the mass $m(t)$ of the ballast chamber is approximately 0.25 Kg whereas it was initialized to a value of about 10^{-2} Kg.

The results for the three kind of diving maneuvers listed above are reported in Figs. 6–8. The ramp simulation case shows, in particular, that in compliance with the complementary design of the solution the motors effort goes to zero asymptotically while delivering a significant contribution during the early phase of the maneuver. The ballast chamber activity, to the contrary, is persistent over a long time interval. The simulation in Fig. 8 clearly demonstrates the ability of the solution to achieve automatic buoyancy calibration and it also confirms that the thrusters activity is mostly concentrated at high frequency.

The behavior of the proposed solution is compared to two alternatives: the first consists in simply using one of the two actuation systems. This is what actually occurs using the factory designed depth control system that allows to select either the electrical thrusters or the ballast chamber during a given mission. The same experiment illustrated in Fig. 6 is executed using the thruster only as commanded through the same PID controller implemented in the complementary control case. The results of this simulation are depicted in Fig. 9. The convergence to the reference path is much slower than when using the complementary solution and, as a consequence of the positive buoyancy calibration, the thrusters effort is significantly larger (and saturates). At last, in order to evaluate the performance of the proposed approach as opposed to an alternative reliable solution, a feedforward/feedback solution has been implemented. The structure of this control architecture is schematically depicted in Fig. 10. This is a well-known schema also known as two degree of freedom architecture. The feedback component, when properly designed, guarantees robustness to model uncertainties, output and matched disturbances while the feedforward term acts as an open loop command able to eventually limit the feedback control effort. The feedforward command is computed by implementing a stable and proper estimate of the plant inverse. With reference to Eq. (37), using the ballast chamber actuation system to implement the feedforward command, this results in

$$U_1(s) = F(s)\, Z_d(s), \tag{48}$$

$$F(s) = \frac{s(\tilde{M}s + \beta)(s + k)}{g(s + 1)^3}, \tag{49}$$

where $Z_d(s)$ is the depth reference and the poles of $F(s)$ are fixed in -1 given that its zeros act at much lower frequencies. As a consequence $F(s)$ approximates the inverse of Y/U_1 in Eq. (37) on the relevant frequencies.

https://doi.org/10.1017/S0263574715000119 Published online by Cambridge University Press

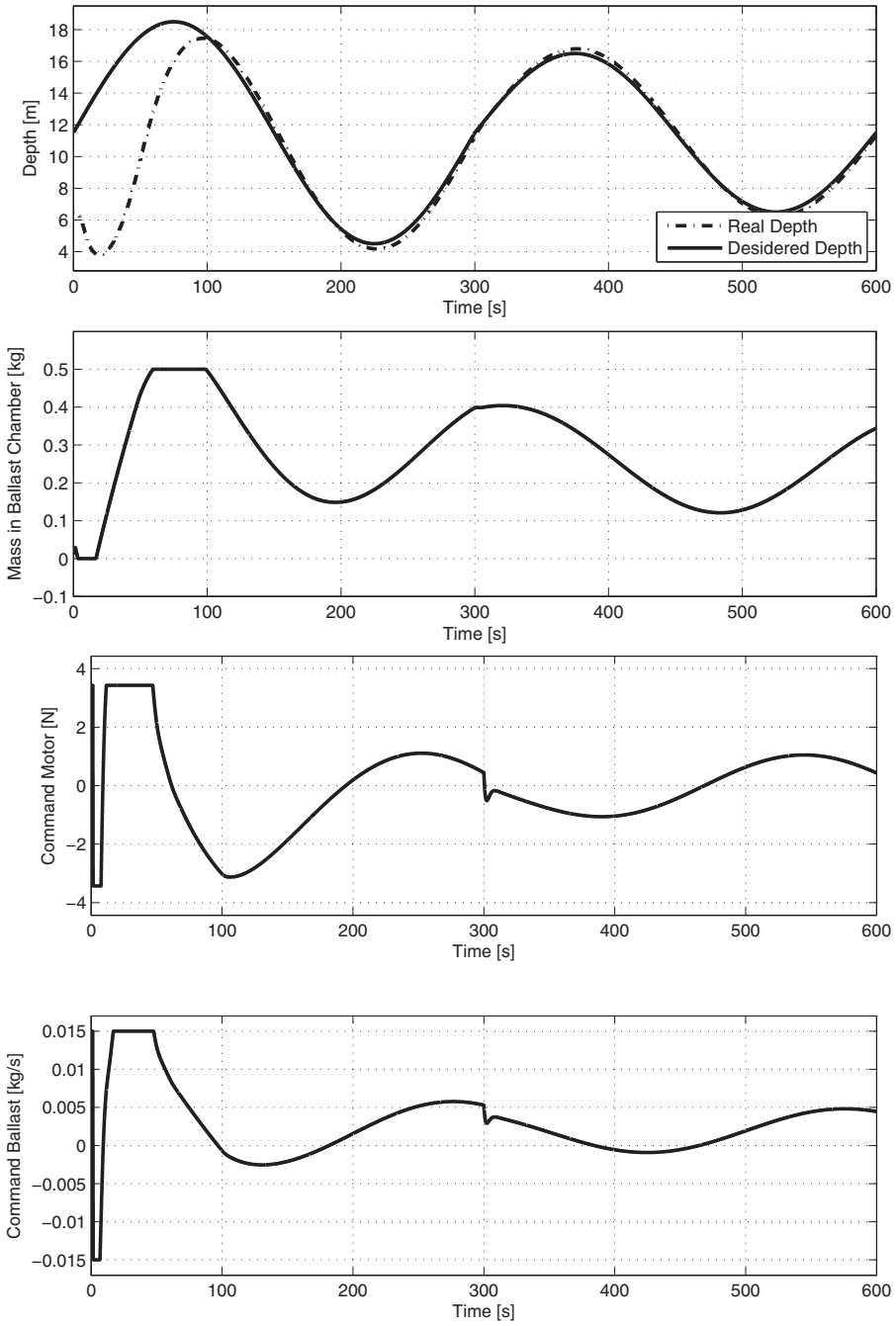


Fig. 6. Complementary control of depth: sinusoidal depth reference with amplitude 7m until $t = 300$ s and 5 m afterwards. The u_2 motor thruster command and u_1 ballast chamber commands are in the two bottom plots.

The feedback controller in Fig. 10 refers to the electrical thrusters and it is actually the same PID of Eq. (41) adopted for the complementary solution, but its output is now fed only to the thrusters. Notice that the feedforward/feedback solution does not lead to neutrally buoyant calibration as the open loop action of the ballast chamber is model based, hence there is no way that it can "learn" how to balance weight and buoyancy if this information is not encoded in the model. Hence, unless the vehicle is initially neutral (which is not the case in the presented simulations and in most practical cases) the open loop command will not counteract this effect. In technical terms this situation is reflected by the fact that $F(s)$ (being an estimate of the inverse of Y/U_1) has a zero in the origin. Indeed, notice that the ballast chamber control effort in Figs. 11 and 12 is mostly

https://doi.org/10.1017/S0263574715000119 Published online by Cambridge University Press

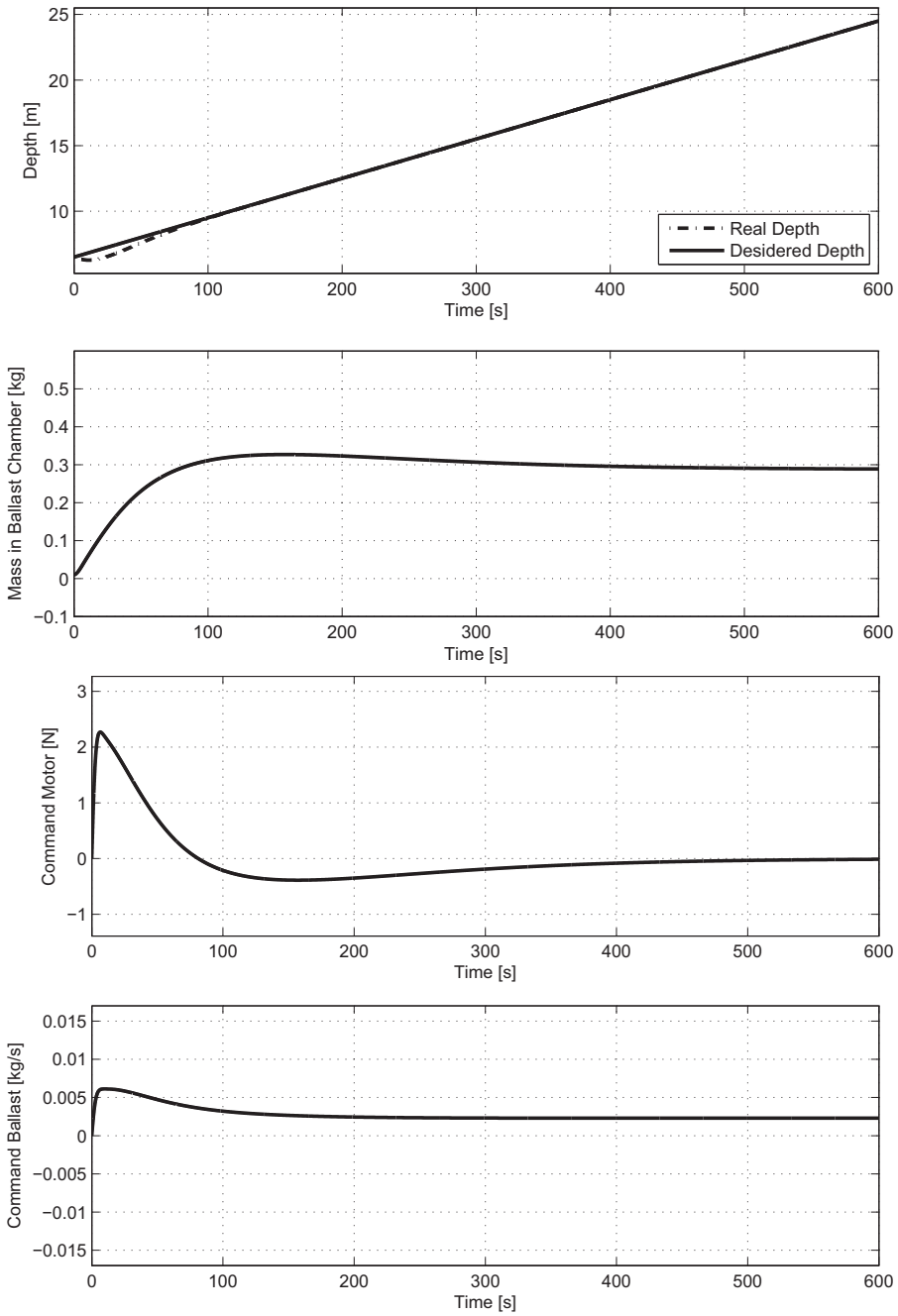


Fig. 7. Complementary control of depth: ramp depth reference.The u_2 motor thruster command and u_1 ballast chamber commands are in the two bottom plots.

concentrated at high frequencies. As a consequence the thrusters are also active at low frequencies as opposed to the desired behavior that is indeed achieved through the proposed complementary solution.

6. Conclusion

The basic frequency based methods known as complementary filtering have been revised for signal sensor processing and linear state space estimation. The complementary filtering paradigm has been extended to the design of a control system for an actuator redundant robot. The proposed

https://doi.org/10.1017/S0263574715000119 Published online by Cambridge University Press

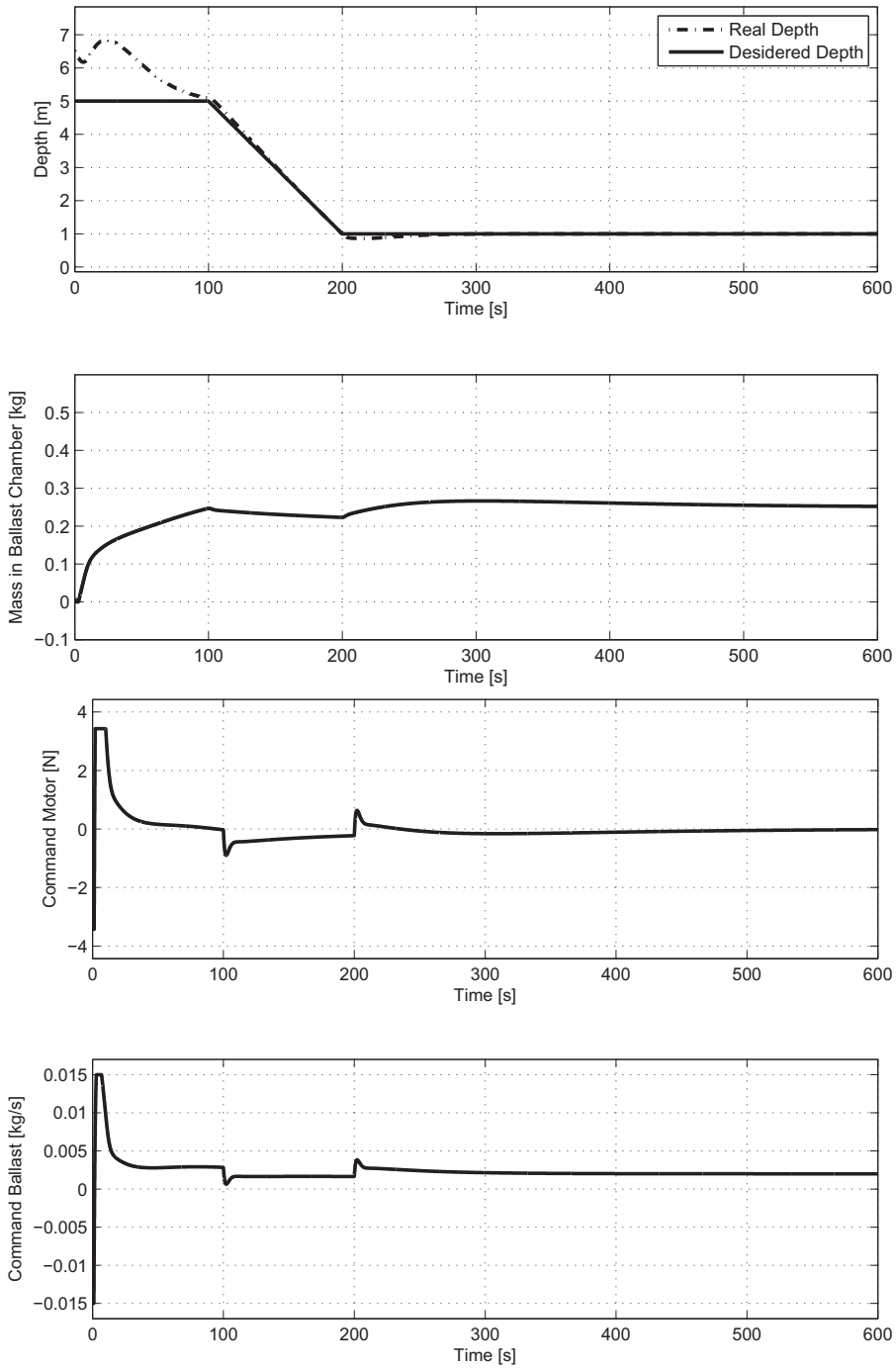


Fig. 8. Complementary control of depth: dive maneuver as in ref. [3]. The u_2 motor thruster command and u_1 ballast chamber commands are in the two bottom plots.

approach is applicable to all situations where a given plant degree of freedom is controlled by different actuation systems with complementary bandwidths. In particular, the solution is of possible interest for robots with redundant actuators. The advantage of using complementary filtering for controller design in the presence of redundant actuation systems is that classical and well-known frequency methods can be fully exploited to allow the actuators to work in their natural frequency spectrum: the overall necessary feedback control action can be designed based on any desired methodology. Once the overall actuation output has been determined, this can be generated distributing

https://doi.org/10.1017/S0263574715000119 Published online by Cambridge University Press

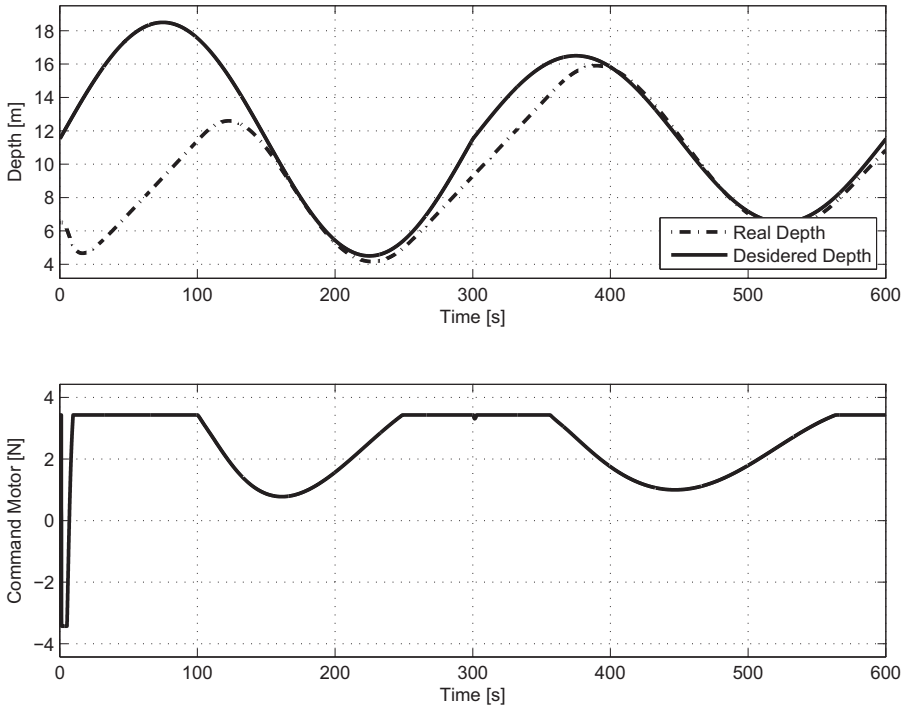


Fig. 9. Thrusters only depth control: sinusoidal depth reference as the one in Fig. 6.

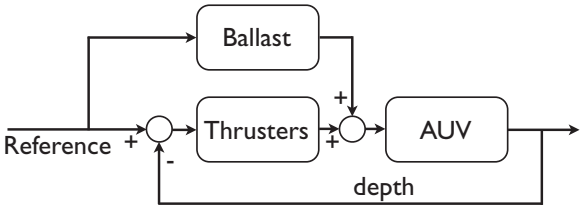


Fig. 10. Alternative feedforward/feedback architecture for the heave control exploiting the given actuator redundancy. Refer to the text for details.

the control effort on the available actuators based on their specific dynamics. The definition of such control effort distribution policy is done in the frequency domain: contrary to alternative state space methods to address the thruster allocation problem, the described complementary control approach allows the designer to fully exploit the knowledge of the frequency domain actuator model. As a result, the available actuation systems operate concurrently each working in their most natural spectrum.

As a specific application, the depth control of an AUV having two actuator systems for the heave degree of freedom has been addressed: the two actuation systems are (i) a ballast tank that can be filled or emptied changing the restoring force acting on the vehicle and (ii) a set of vertical jet thrusters generating a vertical force. These two actuation systems have different dynamic behaviors: while the ballast tank system is relatively slow, the vertical jet thrusters have a much faster response. A single PID controller (implemented through an anti-windup architecture) is designed for the necessary vertical force to be generated in order to follow a depth profile. Such desired vertical force is decomposed in two signals corresponding to a lower frequency term and a (complementary) higher frequency one. The former is then generated through the ballast tank actuation system while the latter is generated by the electrically powered vertical thrusters. As a result, the desired vertical force is seemingly generated by the concurrent operation of both actuation system each working in its most natural frequency spectrum. This is opposed to the factory built controller that uses either the ballast tank or the vertical thrusters to control the heave axis according to the mission specifications. The

https://doi.org/10.1017/S0263574715000119 Published online by Cambridge University Press

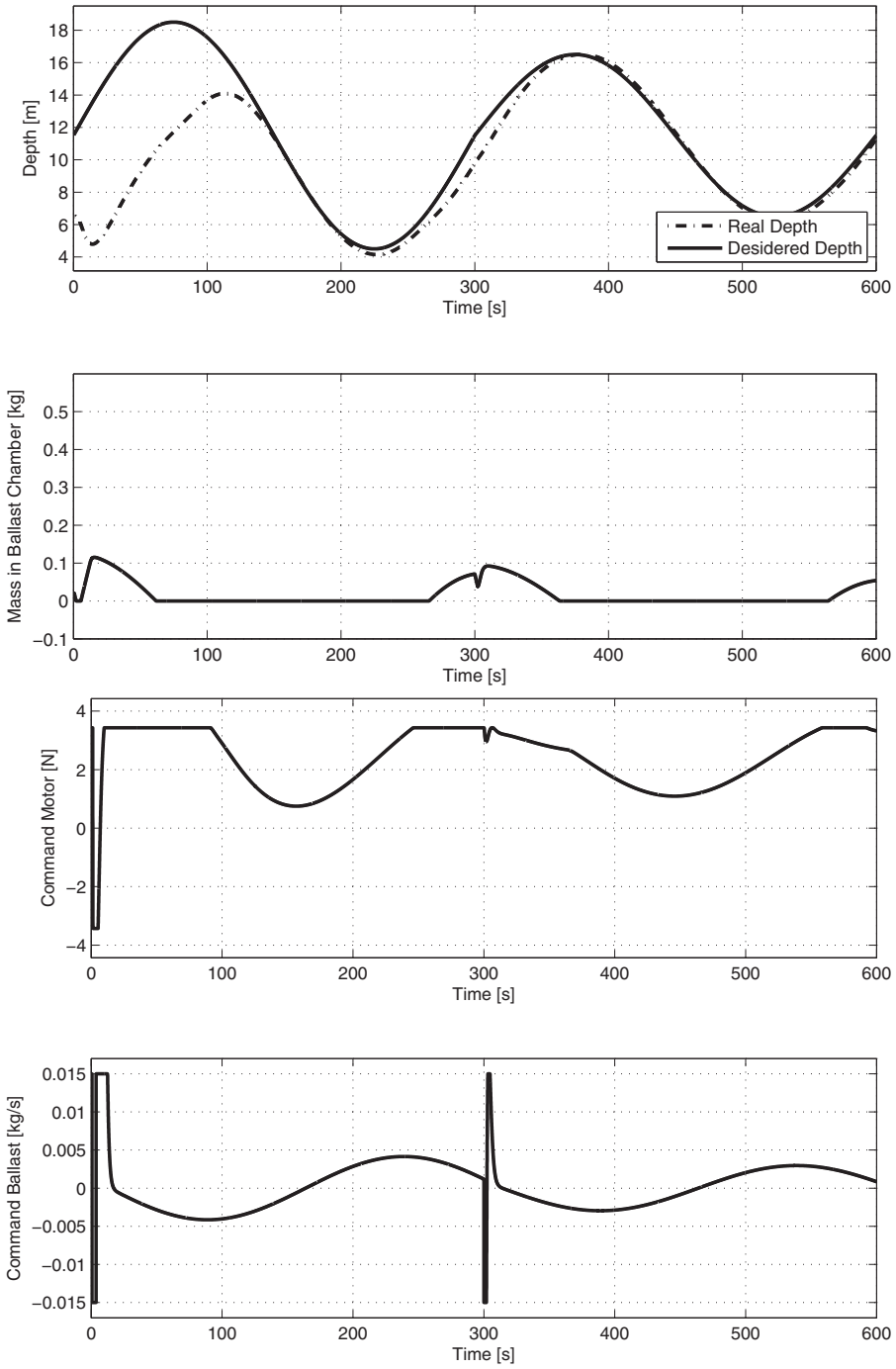


Fig. 11. Feedforward/feedback control of depth: sinusoidal depth reference as in the case of Figs. 6 and 9. The u_2 motor thruster command and u_1 ballast chamber commands are in the two bottom plots.

proposed solution is very simple in terms of realization and it has been proven to be effective in simulation. Given that the integral action of the designed PID controller is basically implemented by the ballast tank system, if the reference depth is constant the proposed solution leads to an automatic neutrally buoyant calibration of the vehicle that, otherwise, needs to be obtained manually prior to starting the mission.

https://doi.org/10.1017/S0263574715000119 Published online by Cambridge University Press

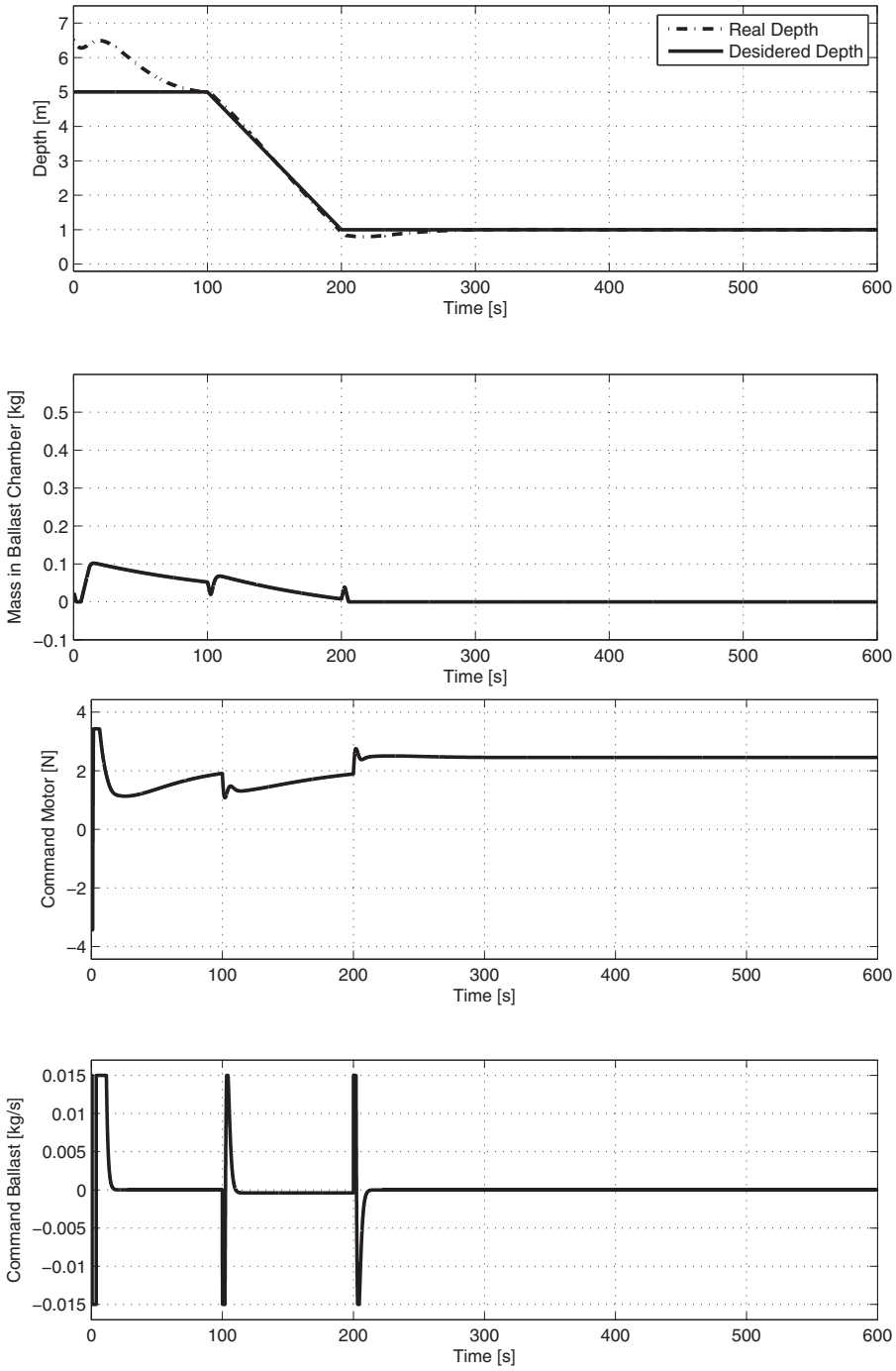


Fig. 12. Feedforward/feedback control of depth: dive maneuver as in ref. [3]. The u_2 motor thruster command and u_1 ballast chamber commands are in the two bottom plots.

Acknowledgments

This work was partially supported by MIUR (Italian Ministry of Education, Universities and Research) under the PRIN project MARIS: Marine Autonomous Robotics for InterventionS, call of year 2010–2011, prot. 2010FBLHRJ. The authors thank the anonymous reviewers for their constructive comments and suggestions.

https://doi.org/10.1017/S0263574715000119 Published online by Cambridge University Press

References

1. A. Alvarez, A. Caffaz, A. Caiti, G. Casalino, L. Gualdesi, A. Turetta and R. Viviani, "Folaga: A low-cost autonomous underwater vehicle combining glider and AUV capabilities," *Ocean Eng.* **36**, 24–38 (2008).
2. K. Åström and T. Hägglund, *PID Controllers: Theory, Design, and Tuning*, 2nd ed. (ISA: The Instrumentation, Systems, and Automation Society, USA, 1995).
3. M. Caccia, R. Bono, G. Bruzzone and G. Veruggio, "Bottom-following for remotely operated vehicles," *Control Eng. Pract.* **11**, 461–470 (2003).
4. A. Caffaz, A. Caiti, G. Casalino and A. Turetta, "The hybrid glider/AUV folaga," *IEEE Robot. Autom. Mag.* **17**(1), 31–44 (2010).
5. R. Cristi, F. A. Papoulias and A. J. Healey, "Adaptive sliding mode control of autonomous underwater vehicles in the dive plane," *IEEE J. Ocean. Eng.* **15**(3), 152–160 (1990).
6. T. I. Fossen, *Guidance and Control of Ocean Vehicles*, 1st ed. (Wiley, England, 1994).
7. O. Härkegård and S. T. Glad, "Resolving actuator redundancy – optimal control versus control allocation," *Automatica* **41**(1), 137–144 (2005).
8. W. Higgins, "A comparison of complementary and Kalman filtering," *IEEE Trans. Aerospace Electron. Syst.* **AES-11**(3), 321–325 (1975).
9. R. Kurtz and V. Hayward, "Multiple-goal kinematic optimization of a parallel spherical mechanism with actuator redundancy," *IEEE Trans. Robot. Autom.* **8**(5), 644–651 (1992).
10. C. F. Lin, *Modern Navigation, Guidance, and Control Processing*, (Prentice Hall, USA, 1991).
11. R. Mahony, T. Hamel and J. M. Pflimlin, "Nonlinear complementary filters on the special orthogonal group," *IEEE Trans. Autom. Control* **53**(5), 1203–1218 (2008).
12. A. Malerba and G. Indiveri "Complementary Control of the Depth of an Underwater Robot," *Proceedings of the 2014 IFAC World Congress*, IFAC, Cape Town, South Africa, vol. 19 (2014) pp. 8971–8976.
13. V. Salvucci, Y. Kimura, S. Oh, T. Koseki and Y. Hori, "Comparing approaches for actuator redundancy resolution in biarticularly-actuated robot arms," *IEEE/ASME Trans. Mechatronics* **19**(2), 765–776 (2014).
14. C. Silvestre and A. Pascoal "Depth control of the INFANTE AUV using gain-scheduled reduced order output feedback," *Control Eng. Pract.* **15**(7), 883–895 (2007).
15. O. Sørdalen, "Optimal thrust allocation for marine vessels," *Control Eng. Pract.* **5**(9), 1223–1231 (1997).
16. L. V. Steenson, L. Wang, A. B. Phillips, S. R. Turnock, M. E. Furlong and E. Rogers, "Experimentally Verified Depth Regulation for AUVs using Constrained Model Predictive Control," *Proceedings of the 2014 IFAC World Congress*, IFAC, Cape Town, South Africa, vol. 19 (2014) pp. 11974–11979.
17. S. Zanoli and G. Conte "Remotely operated vehicle depth control," *Control Eng. Pract.* **11**, 453–459.

https://doi.org/10.1017/S0263574715000119 Published online by Cambridge University Press